THE
PHYSICAL REVIEW

A journal of experimental and theoretical physics established by E. L. Nichols in 1893

SECOND SERIES, VOL. 188, No. 4 20 DECEMBER 1969

Quasifree p-n Scattering in Deuteron Breakup Induced by 46-MeV Protons*

E. L. PETERSEN†

Department of Physics, San Fernando Valley State College, Northridge, California

AND

R. BONDELID

Naval Research Laboratory, Washington, D. C. and Department of Physics, University of California, Los Angeles, California 90024

AND

P. TOMAŠ,‡ G. PAIĆ,§ J. REGINALD RICHARDSON, AND J. W. VERBA

Department of Physics, University of California, Los Angeles, California 90024

(Received 28 July 1969)

The disintegration of deuterons by protons was investigated in a kinematically complete experiment detecting neutrons and protons. Measurements were made at 42 different pairs of angles, in and out of the scattering plane, using an associated charged-particle time-of-flight technique and a proton counter telescope. Experimental results are compared with spectator-model calculations, using the impulse approximation, and a Chew-Low extrapolation is presented. At a few sets of angles the n-p final-state interaction was observed.

INTRODUCTION

THE nucleon-deuteron (N-D) interaction in many aspects represents the simplest "complicated" system that can be studied with the hope that the results can be given an exact interpretation in the near future. The accumulated experimental evidence for the p-D interaction, using incident protons of widely varying energies, has indicated that these are two dominant processes: (a) the process involving the final-state interaction (FSI) of two nucleons (np or pp), and (b) a direct process involving the scattering from one nucleon with the remaining nucleon almost unaffected by the process, i.e., quasifree scattering (QFS). Process (a) has been extensively investigated to obtain information about the low-energy N-N scattering parameters.[1] Process (b) has not been studied extensively in the p-D system, although the process has been widely used for spectroscopic studies on heavier nuclei. It seemed to us that the general lack of data on the QFS of nucleons from the deuteron, the apparent disagreement between $D(p, 2p)$ experiments at different energies,[2–7] and the lack of proton-neutron cor-

* Work supported in part by the U. S. Atomic Energy Commission.

† Present address: Oberlin College, Oberlin, Ohio.

‡ Present address: Institute "R. Bošković," Zagreb, Yugoslavia.

§ On leave of absence from Institute "R. Bošković," Zagreb, Yugoslavia.

[1] See, e. g., W. T. H. van Oers and I. Šlaus, Phys. Rev. **160**, 853 (1967); W. T. H. van Oers (unpublished); also H. Brückman, W. Kluge, and L. Schänzler, Phys. Letters **24B**, 649 (1967).

[2] A. F. Kuckes, R. Wilson, and R. F. Cooper, Jr., Ann. Phys. (N. Y.) **15**, 137 (1961).

[3] R. E. Warner, Phys. Rev. **132**, 2621 (1963).

[4] S. M. Bunch, C. C. Kim, and H. H. Forster, Rev. Mod. Phys. **37**, 528 (1965).

[5] K. Kuroda, F. Takeuchi, and T. Yuasa, in Proceedings of the International Conference on Nuclear Structure, Tokyo, 1967 (unpublished).

[6] I. Slaus, J. W. Verba, J. R. Richardson, R. F. Carlson, L. S. August, and E. L. Petersen, Phys. Letters **23**, 358 (1966).

[7] B. Kuhn, H. Kumpf, K. Möller, and J. Mösner, in *Few Body Problems, Light Nuclei and Nuclear Interactions*, edited by G. Paić and I. Šlaus (Gordon and Breach, Science Publishers, Inc., New York, 1969); B. Kuhn, H. Kumpf, K. Möller, and J. Mösner, Nucl. Phys. **A120**, 285 (1968).

Copyright © 1970 by The American Physical Society

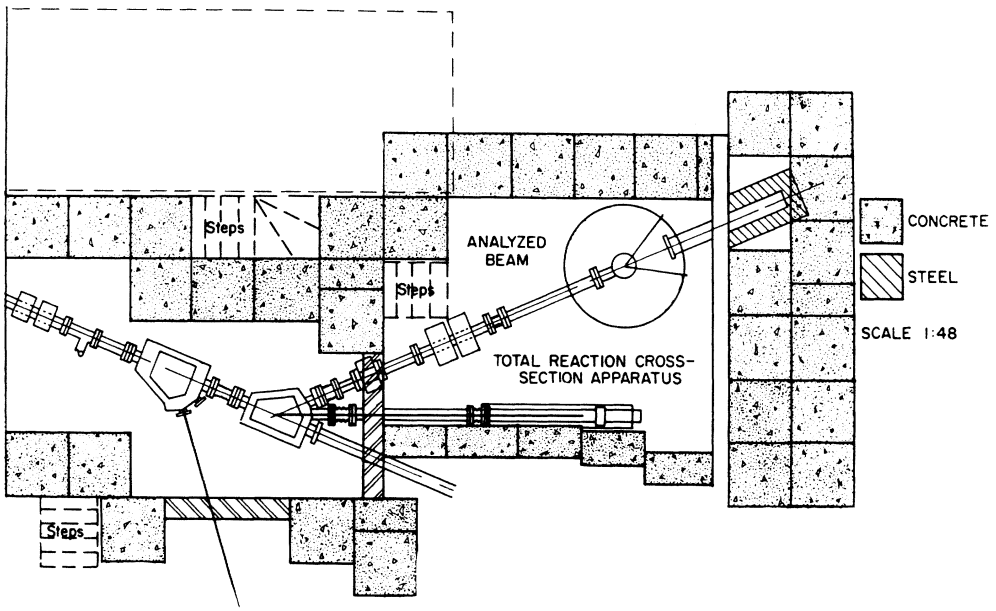

FIG. 1. Layout of the experimental area.

relation measurements justify the measurement of the $D(p, pn)p$ reaction in that region of momentum space where the maximum contribution to the QFS process can be expected. From the experimental point of view, the neutron-proton correlation experiment has advantages over the proton-proton correlations. These lie in the fact that p-p, but not n-p, coincidences can be caused by the hydrogen contamination in the target, and in the fact that the detection of low-energy neutrons is easier than that of low-energy protons. The measurement of the p-n correlation spectra provides two important pieces of information relevant to the study of the QFS process: (1) the absolute magnitude of the cross section and (2) the shape of the spectra. The existing $(p, 2p)$ data have indicated substantial departures from the predictions on both points. We concentrate on the measurement of spectra at different sets of angles, changing thereby the basic parameters in the QFS analysis. In addition, one series of measurements was made where we moved one counter out of the horizontal plane in order to compare the noncoplanar results with the theoretical predictions.

Proton-neutron correlation spectra have been measured at 42 different sets of angles in and out of the scattering plane. Several sets of angles were chosen so as to favor the emission of n-p pairs with low relative momentum to see the effect of the FSI process and its importance relative to the QFS.

EXPERIMENTAL TECHNIQUE AND DATA ANALYSIS

In neutron-proton correlation experiments, it is necessary to pay particular attention to accidental counts arising from the γ-ray and neutron background. The primary approach is to remove or shield all sources of such background. In our experiment, the target (15-mg/cm^2 deuterated polyethylene) is placed in a vacuum chamber, and the experimental area is arranged so that the beam (46-MeV protons) cannot hit anything near the target. The beam-defining slits and the Faraday cup are well shielded, as shown in Fig. 1. The beam-handling area is covered with 4.5 in. of steel and 18 in. of concrete to reduce skyshine.

Since the above techniques cannot completely remove neutron and γ-ray background, and do not affect accidental coincidences due to γ rays and neutrons produced in the target, the electronics is arranged to reduce the accidental count rate as much

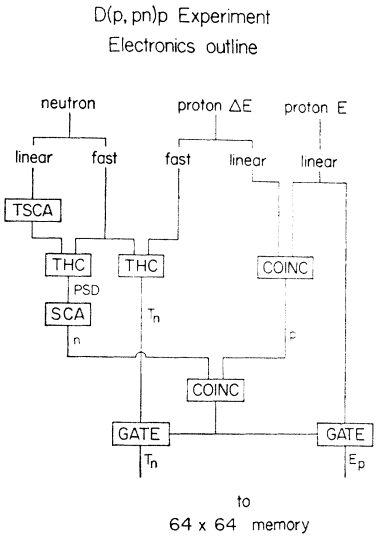

FIG. 2. Simplified block diagram of the electronic circuits.

as possible. Figure 2 shows a block diagram of the electronic arrangement. A time-to-height converter (THC) examines the time between the start of the neutron pulse, as determined by fast crossover, and the slow crossover of the linear signal after a double RC amplifier. This time interval is different for γ-ray pulses and neutron pulses from the 5×5-cm NE213 liquid scintillator. This method of pulse-shape discrimination (PSD) not only works well, but the neutron energy signal and the PSD signal can be displayed on a two-dimensional matrix. This display enables the neutron–γ-ray discriminator to be carefully set so that all neutrons are counted, even if this results in accepting a few low-energy γ rays.

The γ rays in the proton counter are eliminated by requiring a ΔE-E coincidence between a 10-mil Pilot B plastic scintillator and a NaI(Tl) crystal. The NaI(Tl) crystal gives 1.5% energy resolution for the protons, and the plastic scintillator generates a fast signal that can be used for timing the neutron flight. Experimental time resolutions of 1 nsec are generally obtained. For each set of angles, θ_p (proton angle), θ_n (neutron angle), and ϕ_{np} (the angle between the proton and neutron scattering planes), coincident events between one of the outgoing protons and the neutron are recorded in a 64×64 two-dimensional array, energy (proton) versus time of flight (neutron). The counts are accumulated in the memory of an SDS 925 on-line computer. After each run, the total counts are transferred to magnetic tape for later analysis using an IBM 360-75 computer. Circuit delays and timing are introduced to guarantee that the maximum and minimum detectable neutron energies are contained within the boundaries of the 64×64 array.

Even though non-target-associated background is virtually eliminated, there are still accidental coincidences due to events in the target. Since the time of flight is recorded, these accidentals can be easily subtracted by examining the number of counts one or two beam bursts away in time (35 or 70 nsec). In this way the complications of having separate accidental or background runs are avoided. The beam current is then limited solely by the number of target-associated accidentals allowed.

The neutron-detector threshold is set by using the Compton edge of Cs^{137} γ rays. The ratio between the amplitude of the pulse heights for protons and electrons is such that this threshold corresponds to $E_n \simeq$ 2 MeV.[8]

Several geometries are used. The maximum angular acceptance for both counters is always less than $\pm 2°$. The proton-counter solid angles are either 2.95×10^{-3} or 3.65×10^{-3} sr. The proton flight path is usually 40 cm, while the neutron flight path is usually 100 cm. Some measurements are also made with neutron flight paths of 150 and 200 cm. A brass stopper prevents protons from reaching the neutron detector. This stopper could be removed for energy calibration runs using proton-proton scattering. In order to keep the neutron counter in a constant neutron background, we decided to move the proton counter for both the coplanar and out-of-plane measurements.

There are three principal steps in the data reduction program: (1) energy calibration, (2) projection of the cross section on the proton axis, and (3) projection of the cross section on the neutron axis.

The background in the coincidence spectrum shows enhancements from p-d elastic scattering and p-C^{12} elastic and inelastic scattering. These enhancements are used to provide energy calibration information for the proton detector. For most of the runs, the lowest energy obtained from background enhancement is from p-d elastic scattering, and is not less than ~10 MeV. To provide calibration data at lower energies, we perform p-p scattering at relatively large proton-counter angles using a normal polyethylene target. The net energy of the incoming beam at a point halfway through the target is calculated and used to obtain the energy of the elastically scattered protons from hydrogen, and of the elastically and inelastically scattered protons from C^{12}. The energy loss is calculated for the scattered protons in the remainder of the target, for the various foils that separate the target chamber and the proton detector, and for the passing counter.

The angle of the target relative to the incoming beam is set to minimize the loss of energy by protons emerging from the target at different proton-counter angles. Because of the experimental configuration, those elements which cause proton energy loss change in effective thickness with changes in the proton-counter angle. Therefore, the first step in projecting the cross section on the proton energy axis is to create a table of energies with the independent parameter as the energy at the center of the target, in a range assumed to be 1–46 MeV in steps of 0.2 MeV, and the dependent parameter as the energy remaining at the point of entry to the sodium iodide counter. By comparison and interpolation with the previously determined calibration of the proton counter, the actual proton energies and energy intervals as a function of channel number are determined. In contrast to the actual energy calibration, this resulting curve is highly nonlinear and changes with proton-counter angle. It is, therefore, determined individually for each set of experimental angles.

Peak-finding techniques are used to determine the kinematic locus. The enhancement in the background due to the protons elastically scattered from deuterons is always above the proton-channel limit of the kinematic locus (i.e., at higher proton-channel number).

[8] R. Batchelor, W. B. Gillroy, J. B. Parker, and J. M. Towle, Nucl. Instr. Methods **13**, 70 (1961); also, R. J. Schuttler, Oak Ridge National Laboratory Report No. ORNL-3888, 1966 (unpublished).

TABLE I. Efficiency of the neutron counter, calculated for a NE213 liquid scintillator. The scintillator used is a cylinder 5.08 cm long and 5.08 cm in diameter. Threshold neutron energy $E_n = 2$ MeV.

E_n	Efficiency	E_n	Efficiency
2.0	0.0182	11.0	0.1327
2.5	0.1321	11.5	0.1298
3.0	0.1502	12.0	0.1272
3.5	0.1562	12.5	0.1255
4.0	0.1530	13.0	0.1240
4.5	0.1647	13.5	0.1224
5.0	0.1682	14.0	0.1204
5.5	0.1674	14.5	0.1107
6.0	0.1658	15.0	0.1111
6.5	0.1634	16.0	0.1106
7.0	0.1600	17.0	0.1113
7.5	0.1566	18.0	0.1138
8.0	0.1531	20.0	0.1204
8.5	0.1434	22.0	0.1237
9.0	0.1459	25.0	0.1256
9.5	0.1424	30.0	0.1180
10.0	0.1331	34.0	0.1122
10.5	0.1358	38.0	0.1035

In most of the proton channels, the largest number of counts below this occurs along the kinematic locus. Although the number of counts in the background region is generally small, it has been adequate to employ the test of standard deviation to determine the limits of the peak under which the counts are added. Background under the kinematic locus is determined by one of two methods. Because of the pulsed nature of the cyclotron beam, the background data, when projected on the neutron time-of-flight axis, show an enhancement with a period equal to the period of the cyclotron radio frequency. It is, therefore, argued that the background in the spectrum 1 rf cycle from the kinematic locus is the best measure of the background to be subtracted. In the first method of background subtraction, this is done on a channel-by-channel basis. In one important set of runs, an error in timing caused us to miss counts in the first four or five channels, and the last four or five channels of the 64 channels on the time-of-flight axis. In this case, background is determined by examination of the variation of background as a projection on the neutron axis for the region above the *p-d* elastic energy. Although it is expected that the background is made up of a superposition of Gaussian distributions on a general background, it is assumed that this background can be approximated with a cosine curve. Approximate parameters for this assumed cosine curve are determined, and, by renormalization to the background region outside the peaks along the kinematic axis, the background under each peak is calculated and subtracted. The net counts per unit energy interval has thus been determined. Before the cross section can be calculated, however, it is necessary to calculate the neutron-counter efficiency, and to introduce a normalization factor for target thickness and integrated beam current. The neutron time-of-flight axis does not provide an absolute measure of the neutron energy because the total delays in the circuits are not known. However, since the proton energy is known, the neutron energy can be calculated from three-body kinematics. By relating these calculated neutron energies to the peaks along the kinematic locus, the calibration in terms of neutron energy along the neutron axis is provided. A table (Table I) of neutron efficiency versus neutron energy is then used to determine the counter efficiency for each neutron energy. During each run, a monitor counter records the number of protons elastically scattered from the deuterons in the target. Using previously determined absolute cross sections for *p-d* scattering,[9] and the known solid angles, a normalization for each run is obtained. Finally, the projection of the cross section on the proton axis is obtained.

For projection of the cross sections on the neutron axis, similar information to that described above is used. The peak-finding technique is essentially the same, the neutron energies and efficiencies are obtained as described above, background is determined as above, and, using the normalization factor, the cross section is calculated.

The experimental cross sections are subject to several sources of uncertainties, listed in Table II. It is important to point out that most of the quoted uncertainties are dependent on the energy of the observed particles. The uncertainties given in Table I are for energies of particles around 22 MeV.

The solid angle of the neutron detector was cal-

TABLE II. Uncertainties in the determination of the absolute experimental total cross sections. The uncertainties are given for particle energies of about 22 MeV.

Source	Character	Estimated uncertainty effect on the cross section (%)
Solid angle of the neutron counter	Systematic	−2
Neutron-counter efficiency	Systematic	±10
Neutron-counter threshold relative to neutron efficiency	Systematic	±0.5
Neutron energy calibration relative to neutron efficiency	Random	±1
Knowledge of incident beam energy relative to neutron efficiency	Random	±1
Neutron absorption	Systematic	±0.6
Finite geometrical effects	Systematic	±2.5
Monitor-counter position	Systematic	±2
Monitor-counter solid angle	Systematic	±1
Monitor-counter counts	Random	±0.1
Monitor-counter dead time	Random	−1
Uncertainty in measured $D(p, p)D$ cross section	Systematic	±2
Background subtraction	Random	±1

[9] S. N. Bunker, J. M. Cameron, R. F. Carlson, J. Reginald Richardson, P. Tomaš, W. T. H. van Oers, and J. W. Verba, Nucl. Phys. **A113**, 461 (1968).

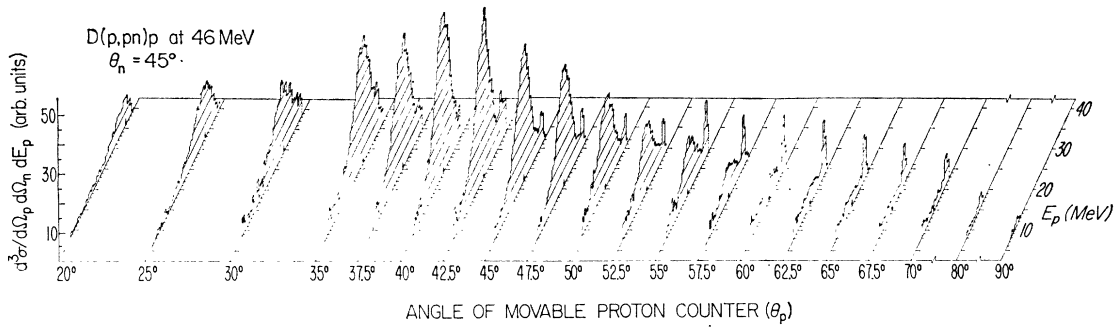

FIG. 3. Proton-neutron correlation spectra projected on the proton energy axis for different angle setting of the proton detector in the scattering plane. The neutron detector was fixed at $\theta = 45°$, while the movable proton detector covered the angular region 20°–90°.

culated using the distance from the target to a point halfway through the scintillator, and it is probable that the effective solid angle is slightly larger. The neutron detection efficiency introduces the most important uncertainty. The efficiencies used in the present experiment are given in Table I, and are calculated using the FORTRAN program of Kurz,[10] modified for the case of NE213. The parameters used in the program were density factor, 0.041; composition of NE213-$CH_{1.213}$; light resolution, 0.13; and threshold energy (equivalent to electrons), 0.589 MeV. The uncertainties here occur primarily in the cross sections used. The uncertainty in the neutron-detector threshold (±100 keV) affects the neutron efficiency in the entire energy range, but primarily at low neutron energies. An uncertainty in the cross section is also introduced by the uncertainty in the neutron energy calibration (500 keV), and the uncertainty in the beam energy (±200 keV) through the shape of the efficiency-versus-energy curve. The uncertainty in the neutron absorption represents the maximum number of neutrons that can be removed by the air, the brass stopper, and the glass window before the neutrons actually reach the liquid scintillator.

The finite geometry effects represent mostly the out-of-plane contributions to the counting rate caused

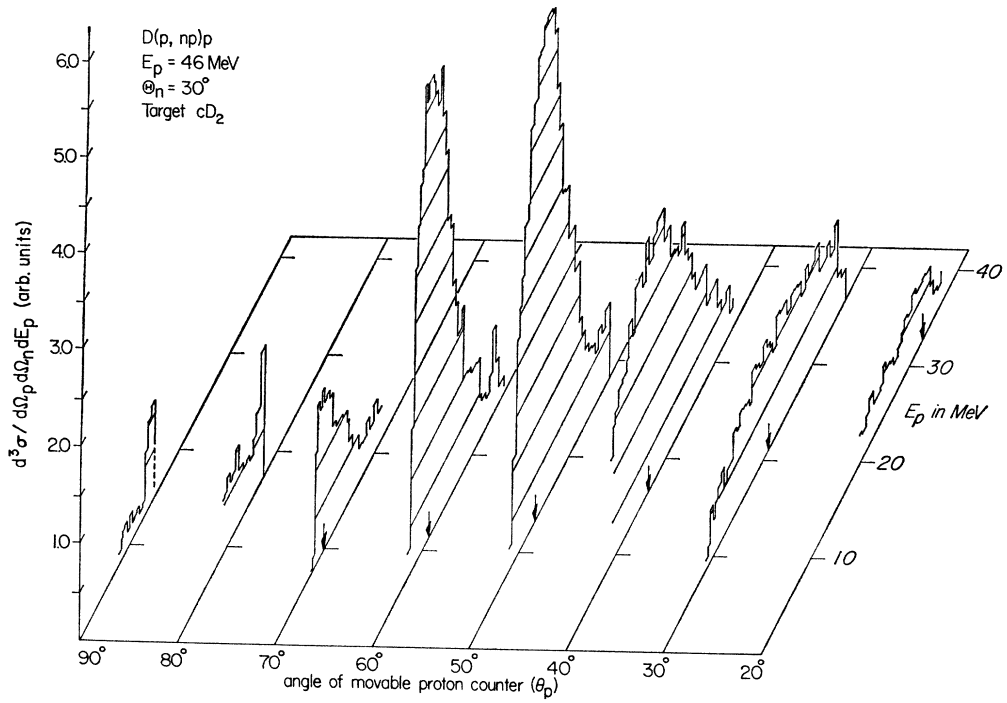

FIG. 4. Same as Fig. 3 except that the neutron detector was fixed at $\theta_n = 30°$. The arrows indicate the position of the minimum spectator energy.

[10] R. J. Kurz, University of California Lawrence Radiation Laboratory Report No. UCRL-11339 (unpublished).

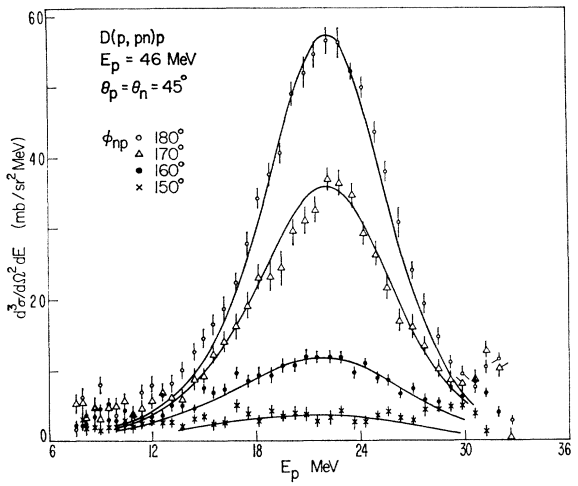

FIG. 5. Noncoplanar neutron-proton correlation spectra for $\theta_n = \theta_p = 45°$ projected on the proton energy axis for $\phi_{np} = 180°$, 170°, 160°, and 150°.

by the height of the detectors and the vertical divergence of the beam (±13 mrad).

Since we used a monitor counter for normalization to obtain the cross sections, errors in its angular position due to setting, to beam walks (±0.4°), and to its distance from the target (±5%) influence the cross sections.

The results obtained in various runs were reproducible in absolute cross section within 10%, and it is our belief that the ±11% absolute uncertainty that one deduces from Table II, combined with a relative uncertainty of typically 6–8%, represents a fair estimate of the precision of this experiment.

EXPERIMENTAL RESULTS

The aim of this experiment is primarily the study of *n-p* QFS. Extensive measurements are made by varying the proton-counter position through a wide range of angles, keeping the neutron counter at two angles, 45° and 30°. Also, out-of-plane measurements are obtained by keeping the angles of both counters at 45° relative to the incoming beam, but changing the angle between the two scattering planes from 180° to 90°.

A general and most prominent feature of the observed spectra is a distinct enhancement in the spectra at the positions where the energy of the unobserved (spectator) particle is a minimum for a given kinematical situation; and the enhancement increases as the minimum spectator energy decreases. This feature can be seen in the isometric projections presented in Figs. 3 and 4. Because of rather high cutoff energy in the proton telescope (8 MeV), the spectra in Figs. 3 and 4 do not clearly exhibit the enhancements due to the interaction in the final state of the two protons. The high-energy peaks are mainly due to phase-space enhancements, but may also include final-state *n-p* effects. Not surprisingly, the same patterns are visible in the noncoplanar spectra, as shown in Fig. 5 for different values of ϕ_{np}.

The data are compared with a calculation using the simple-impulse-approximation (SIA) cross section given by Kuckes, Wilson, and Cooper.[2] The principal feature of this treatment is that it assumes that the incident nucleon interacts with only one nucleon in the deuteron, and that the nucleons are represented in the final state by plane waves. Instead of calculating the nucleon-nucleon off-energy-shell scattering amplitude, the amplitudes for the elastic and quasifree scattering in plane-wave Born approximation are compared and, finally, the QFS cross section is expressed in terms of the elastic cross section in the following manner[2,3]:

$$\frac{d^3\sigma}{d\Omega_n d\Omega_p dE_p} = \frac{4\sqrt{2}}{\pi^2} \frac{(\sqrt{E_\alpha}+\sqrt{E_\beta})^3(\sqrt{E_\alpha E_\beta})^{1/2}}{(\sqrt{E_0})(E_\alpha+2E_s)^2(E_\beta+2E_s)^2} \times \frac{E_n(\sqrt{E_p})\sigma(\theta, E)}{2(\sqrt{E_n})-(\sqrt{E_0})\cos\theta_n+(\sqrt{E_p})\cos\theta_{np}} \quad (1)$$

In this expression, $E_\alpha = 2.226$ MeV and $E_\beta = 59.8$ MeV are the parameters of the Hulthén wave function representing the deuteron, E_0 is the incident proton energy, E_n, E_p, and E_s are the energies of the scattered neutron, proton, and spectator proton, respectively, θ_n is the scattering angle of the neutron, and θ_{np} represents the angle included between the neutron and proton counter in the plane determined by them and the target. The definition of θ_{np}, as given below, allows the use of the Eq. (1) for coplanar and noncoplanar geometries:

$$\cos\theta_{np} = \cos\theta_n \cos\theta_p + \sin\theta_p \sin\theta_n \cos\phi_{np}, \quad (2)$$

where θ_p is the proton scattering angle. The quantity $\sigma(\theta, E)$ represents the on-energy-shell differential cross section for neutron-proton elastic scattering in the center-of-mass system. The center-of-mass angle θ changes with θ_n and θ_p, unless $\theta_n = \theta_p$, when $\theta = 90°$. However, because of the rather small variation of $\sigma(\theta, E)$ with angle, we have used in all our calculations data for $\theta = 90°$. The energy E, which represents the energy of a proton bombarding a neutron at rest, is equivalent to the energy available in the center-of-mass system of the detected proton and neutron in the three-body exit channel of the $D(p, pn)p$ reaction. The energy E, given in a relativistic calculation by

$$E = (1/M_n)[E_n E_p + E_p M_n + E_n M_p - (E_n^2+2E_n M_n)^{1/2}(E_p^2+2E_p M_p)^{1/2}\cos\theta_{np}], \quad (3)$$

varies considerably with angle, thus changing the value of $\sigma(\theta, E)$ to be used at a given pair of angles. For instance, in the case of θ_p ranging from 20° to 80°

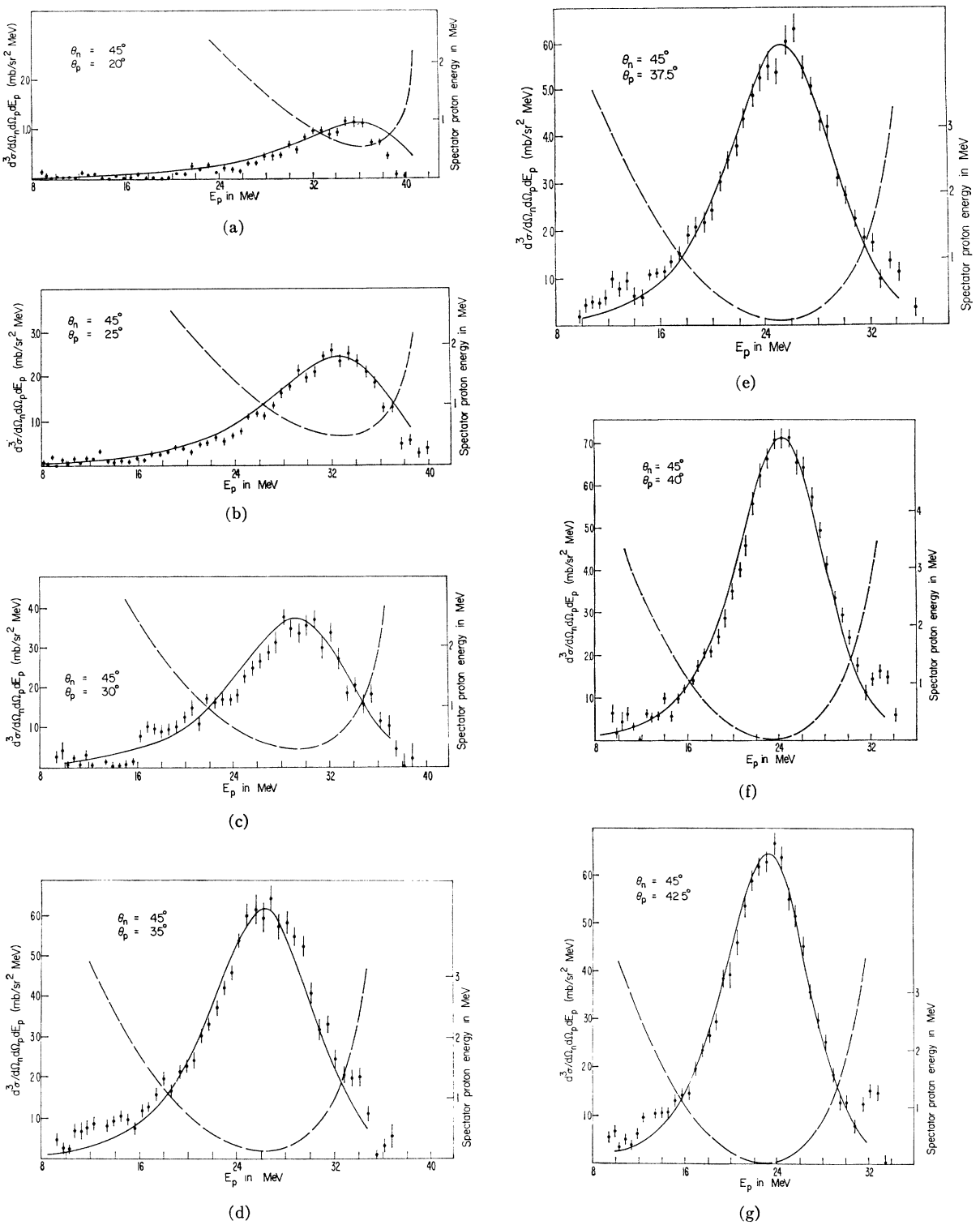

FIG. 6. Coplanar neutron-proton correlation spectra projected on the proton energy axis for $\theta = 45°$ and the θ_p values indicated on the figures. The solid curves represent the result of a SIA calculation normalized to the data. The error bars represent statistical errors only. The dashed curves represent the variation of the spectator energy.

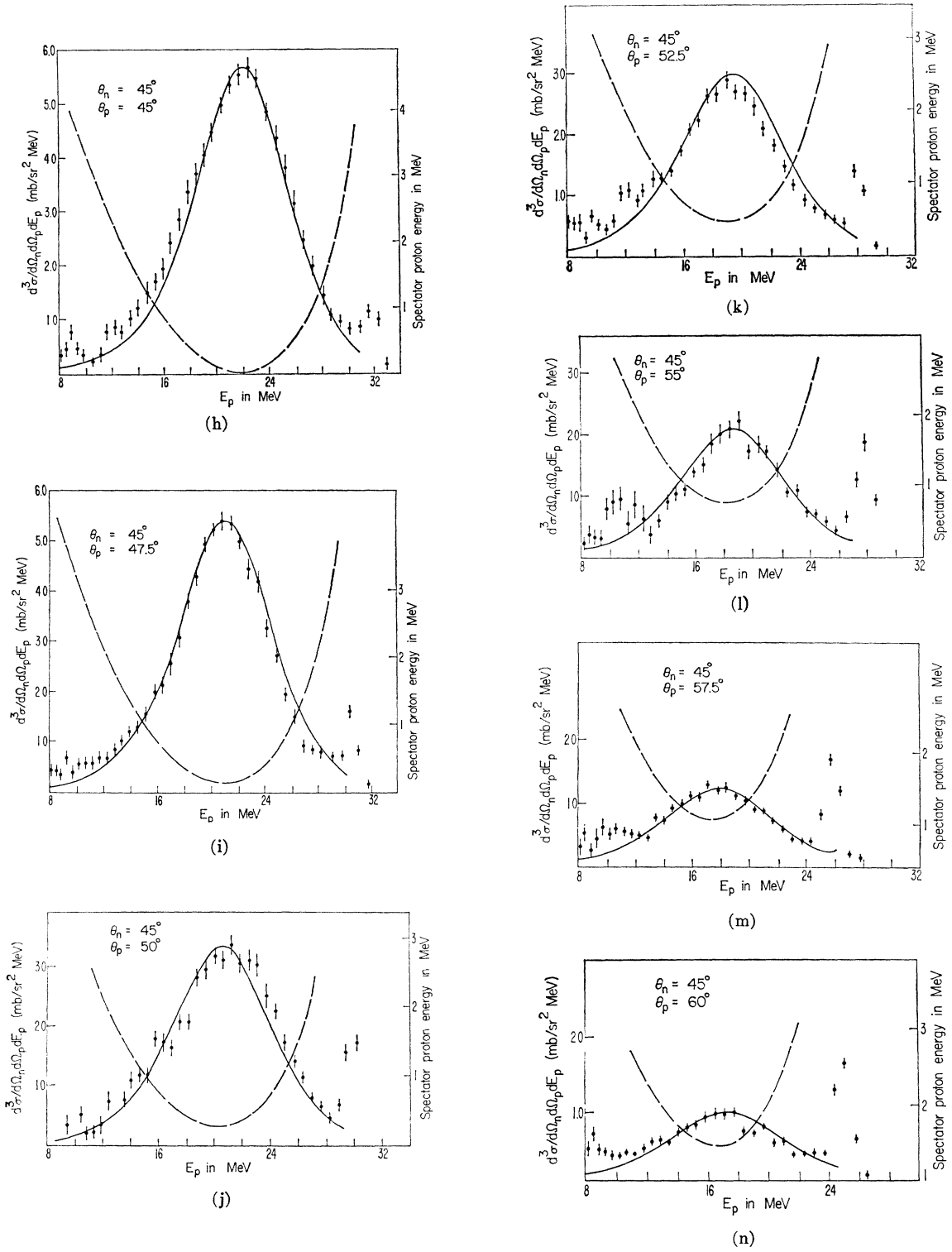

FIG. 6. (*Continued*).

with $\theta_n=45°$, the center-of-mass energy in the n-p system varies from 14.8 to 28 MeV, which means the use of $\sigma(\theta, E)$ values ranging from ~25 to ~10 mb/sr. The fit obtained at different angles θ_p keeping θ_n constant is represented in Figs. 6(a)–6(p). These fits are obtained by normalization to the peaks. The fits

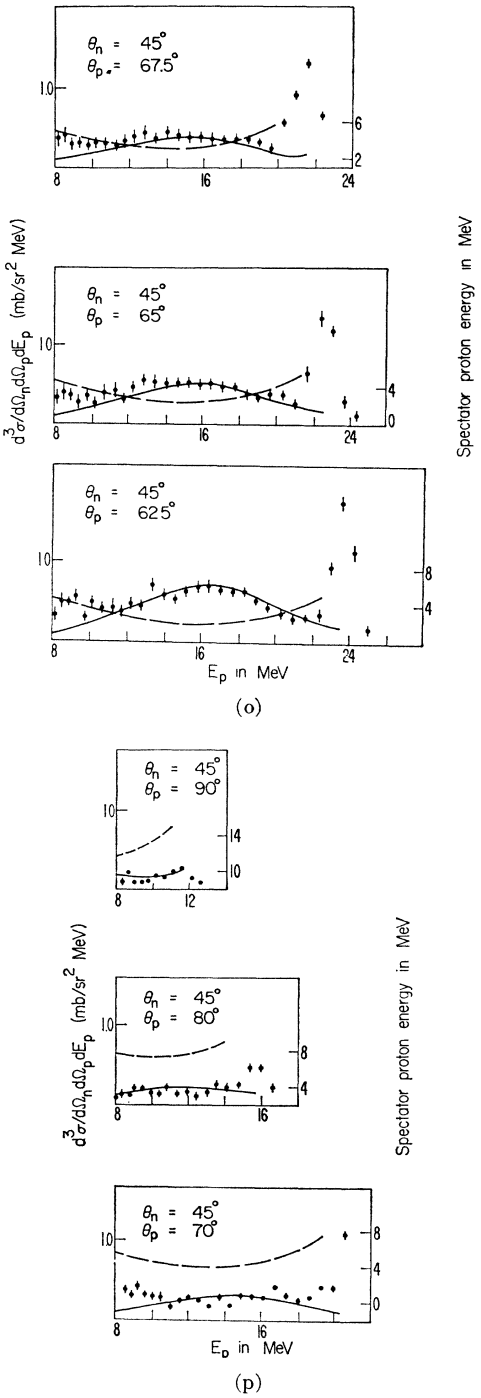

FIG. 6. (*Continued*).

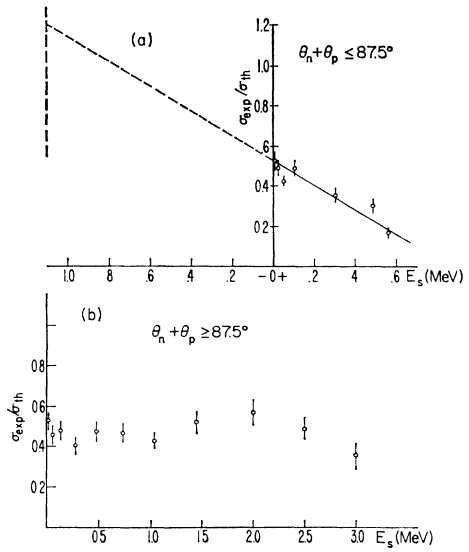

FIG. 7. Ratio $\sigma_{\text{expt}}/\sigma_{\text{theor}}$ for the maximum cross sections, measured varying θ_p and keeping $\theta_n=45°$, plotted as a function of the energy of the unobserved particle. The line drawn in Fig. 7(a) was obtained by a least-squares fit.

obtained with $\theta_n=45°$ are good representations of the situation occurring at $\theta_n=30°$, so that the comparison is not shown for $\theta_n=30°$. The simple theory gives a reasonable prediction of the shapes of he cross-section curves up to a spectator energy of about 3 MeV. Listed in Table III are peak cross sections $d^3\sigma/d\Omega_n d\Omega_p dE_p$ measured at the point where the spectator has minimum energy, the calculated energy E [from Eq. (3)], the extrapolated value of $\sigma(\theta, E)$ at $\theta=90°$ from the compilation made by Wilson,[11] the cross section $N=\sigma'(\theta, E)$ actually used in the normalized theoretical fits of Figs. 6(a)–6(p), and the corresponding spectator energy, all of which are expressed as a function of proton angle.

Table III shows a considerable disagreement between the maximum observed cross sections and those given by the theoretical treatment, a disagreement that cannot be explained by the experimental uncertainties. It has been shown by Chew and Low[12] that a disagreement is to be expected for values of the spectator energy lying in the physical region ($E_s>0$). One assumes that the cross section, in a restricted energy range, is dominated by the influence of a pole located at $E_s=-\frac{1}{2}E_\alpha$, and that the on-energy-shell approximation would be fully valid at the pole location. The ratio of experimental to theoretical cross sections calculated in the simple theory should extrapolate to unity for $E_s=-1.1$ MeV. The ratio $\sigma_{\text{expt}}/\sigma_{\text{theor}}$ is shown in Figs. 7(a) and 7(b). The ratios displayed there are those obtained taking the

[11] R. Wilson, *The Nucleon-Nucleon Interaction* (John Wiley & Sons, Inc., New York, 1963).
[12] G. F. Chew and F. E. Low, Phys. Rev. **113**, 1640 (1953).

TABLE III. Values used in the Chew-Low extrapolation.

θ_p (deg)	$(d^3\sigma/d\Omega_n d\Omega_p dE_p)_{max}$ (mb/sr² MeV)	E (MeV)	$\sigma(\theta, E)$ (mb/sr)	N (mb/sr)	E_s (MeV)
20.0	1.2	14.8	25.0	4.30	0.56
25.0	2.4	15.2	24.0	7.28	0.49
30.0	3.7	16.5	21.5	7.70	0.30
35.0	6.0	18.1	18.5	9.80	0.10
37.5	6.1	19.0	17.0	7.20	0.05
40.0	7.1	20.0	15.5	7.60	0.02
42.5	6.4	21.0	14.5	7.80	0.01
45.0	5.5	21.9	13.5	6.22	0.05
47.5	4.9	22.8	13.0	6.25	0.13
50.0	3.3	23.6	12.5	5.05	0.27
52.5	2.9	24.5	12.0	5.70	0.48
55.0	2.2	25.2	11.5	5.50	0.74
57.5	1.3	25.9	11.2	4.70	1.04
60.0	1.0	26.5	10.9	6.65	1.45
62.5	0.8	27.1	10.5	6.05	2.00
65.0	0.5	27.5	10.2	5.05	2.50
67.5	0.4	27.8	10.0	3.60	3.00

maximum cross sections given in Table III and the theoretical cross sections calculated using the $\sigma(E, \theta)$ from Table III. The data are displayed in two groups. Figure 7(a) shows the ratio obtained for data when $\theta_n+\theta_p \leq 87.5°$, and Fig. 7(b) shows that ratio obtained when the sum is greater than 87.5° (at $\theta_n+\theta_p=87.5°$ the energy E_s reaches zero at one point of the spectrum).

The line shown in Fig. 7(a) is the result of a least-squares fit. It is interesting that the line as drawn in Fig. 7(a) intercepts the value $E_s=-1.1$ MeV at a value of the ratio $\sigma_{expt}/\sigma_{theor}$ of 1.2 ± 0.1 instead of 1.0. The uncertainty in the absolute measured cross section ($\pm 11\%$), plus the uncertainty in $\sigma(\theta, E)$, might be responsible for the departure from the unit ratios at $E_s=-1.1$ MeV. However, the ratios shown in Fig. 7(b) cannot be reconciled with the predicted results. The ratios obtained by using integrated cross sections, within the limits $E_s \leq 2$ MeV, show the same feature seen in Figs. 7(a) and 7(b). The Chew-Low plots could also be affected by variations of neutron efficiency with energy. The points for $\theta_n+\theta_p \leq 87.5°$ correspond to a range of neutron energies and efficiencies. However, the use of the efficiencies calculated by Kurz's program should minimize errors of this type. When $\theta_n+\theta_p \geq 87.5°$, the neutrons are observed at essentially constant energy, so that a change in the table of efficiencies would not change the slope of the Chew-Low plot. The results for the case when $\theta_n=30°$ and $\theta_n+\theta_p \leq 87.5°$ are essentially in agreement with the results just presented. In the $\theta_n+\theta_p>87.5°$ region, we have only two points when $\theta=30°$, and it is difficult to give any appraisal on the basis of these two points.

In order to complete the set of data on the $D(p, pn)p$ reaction in the particular part of the momentum space favoring the quasifree n-p scattering, we have also performed noncoplanar measurements of correlation spectra. The spectra obtained at $\theta_n=\theta_p=45°$ and $\phi_{np}=180°$, 170°, 160°, and 150°, together with the curves predicted by the SIA, are shown in Fig. 5, and Fig. 8 shows the peak cross sections in the spectra as a function of the angle between the two scattering planes. The solid curve in Fig. 8 was calculated using the values of the n-p elastic scattering differential cross section as given by Wilson and, subsequently, normalizing the final result by 0.51. The disagreement of the points marked by circles in Fig. 8 with the solid curve at $\phi_{np}=180°$ and 170° stems from the effect of the angular aperture of the counters, which has not been folded into the theoretical treatment. It is surprising that the present calculation reproduces the shape of the experimental curve so well. It should also be pointed out that, up to a spectator energy of $\sim$4 MeV, the ratio of $\sigma_{expt}/\sigma_{theor}$ is constant, much as in the cases in the plane with $\theta_n+\theta_p>87.5°$.

In the course of the measurements, two pairs of angles were picked at which the emission of a singlet n-p pair with zero relative energy is possible. Since the outgoing low-energy protons have energies below the detection threshold, the FSI of the n-p pair is observed in the projections on the neutron axis, where the energy calibration and energy resolution are poorer. The results of the measurements at these two pairs of angles show the presence of both the FSI peak and the QFS peak. It is interesting to point out that the QFS is the predominant process even though we are kinematically removed from the best experimental situation ($\theta_n+\theta_p \simeq 90°$). This feature of the preponderance of the quasifree mode of interaction surprisingly has been confirmed[13] at lower energies in the reaction $D(p, pp)n$ at $E_p=8$–11 MeV where, because of the low energy, and hence large de Broglie wavelength, QFS is not expected to take place.

The experimental spectra are shown in Figs. 9(a)

[13] A. Niiler (private communication).

and 9(b). For comparison, the same figure shows the theoretical spectra obtained from the separate consideration of the QFS and FSI processes. Both curves were independently normalized to the data. The curve fitting the high-energy peak in the spectra was obtained by using Eq. (1), with the difference that the subscripts n and p are exchanged. The shape of the low-energy peak was compared with the Watson-Migdal expression,[14,15] which predicts

$$\frac{d^3\sigma}{d\Omega_n d\Omega_p dE_n} \propto \frac{\rho}{(-1/a+\frac{1}{2}r_0k^2)^2},$$

where ρ is the three-body phase space given by

$$\rho = \frac{(\sqrt{E_n})E_p}{2(\sqrt{E_p})-(\sqrt{E_0})\cos\theta_p+(\sqrt{E_n})\cos\theta_{np}},$$

a is the scattering length, r_0 the effective length, and $k=(m\epsilon/\hbar^2)^{1/2}$. The quantity ϵ refers to the center-of-mass energy of the two-nucleon system, and m is the nucleon mass. The calculations are performed using $a_{np}=-23.678$ F and $r_0=2.515$ F.

A review of Figs. 6(i)–6(o) indicates that both p-p and n-p FSI's are present, although not clearly defined, owing to projection on the wrong axis for clear definition of the n-p case and to the high proton threshold in the p-p case.

Coplanar correlation spectra taken at symmetrical angles $\theta_n=\theta_p$ are shown in Fig. 10. The shapes of the experimental spectra are in good agreement with the predictions of the simple theory. The pair of angles 51°-51° is such that both n-p and p-p final states should be observed. There is evidence for both, but the QFS still predominates.

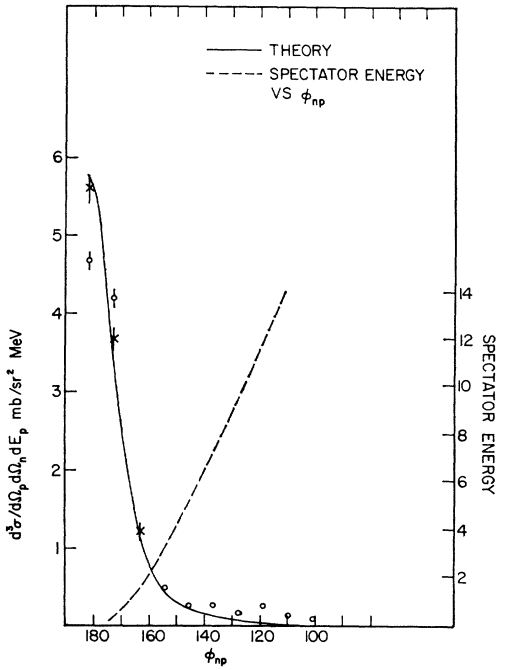

FIG. 8. Peak cross section in the spectra for $\theta_n=\theta_p=45°$ and ϕ_{np} varying from 180° to 90°.

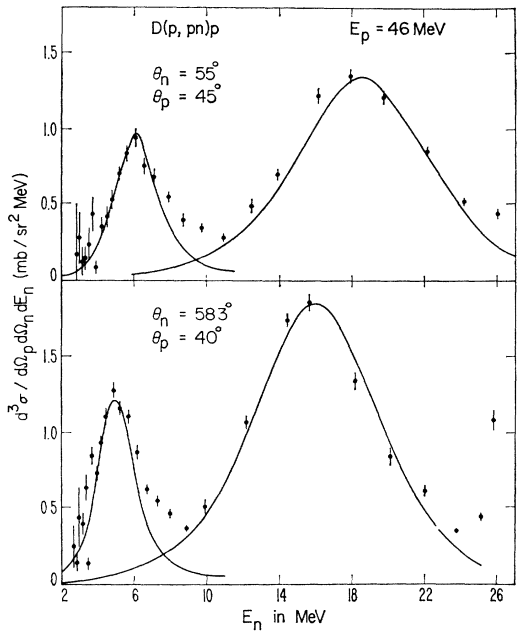

FIG. 9. Proton-neutron correlation spectra projected on the neutron energy axis for two different sets of angles. The theoretical curves have been independently normalized to the data.

DISCUSSION

The observation of both n-p and p-p FSI's suggests that they might partially account for the behavior of the Chew-Low plots, for the data in the plane with $\theta_n=45°$. When θ_p is $<45°$, we are in a kinematic region in which there are no competing processes. However, when $\theta_p>45°$, it seems possible that there are also contributions from the FSI's. Figure 11 shows a kinematic contour plot that demonstrates the various regions. The contours centered at 42.5° and 23 MeV, and extending to 3-MeV spectator energy, indicate the region of QFS.

Figure 11 also shows the contours of internal energy in the final-state p-p and n-p systems. An examination of the data in Fig. 9 indicates that the n-p FSI becomes very weak as the internal energy approaches 2 MeV, and that there is little distortion of the QFS peak. The 2.0-MeV contour of the p-p final state then indicates a rough limit for this effect. Other experiments[16,17] have indicated that the proton-proton FSI does not extend significantly beyond ~4-MeV internal energy. A comparison of Figs. 6(j) and 11 shows no apparent contribution of the p-p FSI past

[14] K. M. Watson, Phys. Rev. **88**, 1163 (1952).
[15] A. B. Migdal, Zh. Eksperim. i Teor. Fiz. **28**, 3 (1955) [English transl.: Soviet Phys.—JETP **1**, 2 (1955)].
[16] B. E. Corey, E. L. Petersen, R. F. Warner, R. W. Bercaw, and J. E. Poth (unpublished.)
[17] C. C. Chang, E. Bar-Avraham, H. H. Forster, C. C. Kim, J. R. Richardson, P. Tomaš, and J. W. Verba, Phys. Letters **28B**, 175 (1968).

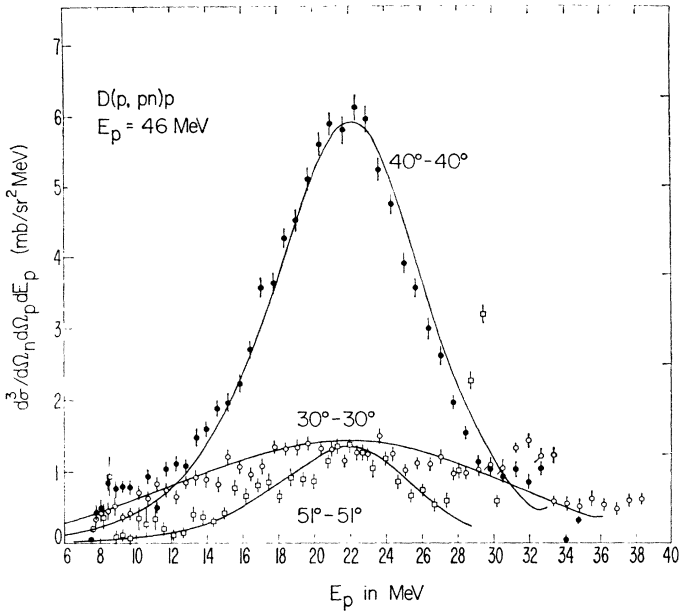

FIG. 10. Coplanar correlation spectra for angles where $\theta_n = \theta_p$.

~4-MeV *p-p* internal energy. However, preliminary calculations by Warner,[18] using the distorted-wave Born-approximation (DWBA) approach of Henley, Richards, and Yu,[19] of only the *p-p* final-state contribution to our results indicates a constant value in the kinematic region dominated by the QFS. This tail, in the range $45° \leq \theta_p \leq 65°$, is about one-half of the (nearly constant) peak cross section at 8-MeV proton energy. If we estimate this contribution from Fig. 6, and subtract it from the QFS peak, there is no significant change in the Chew-Low extrapolation. It does not appear that the FSI's can be directly responsible for the high peak cross section in the region in which $\theta_p > 45°$, and, therefore, for the extraordinary behavior of the Chew-Low plot in this region.

The theoretical treatment has not taken into account the cross-section terms introduced in more sophisticated approaches such as: (a) the Born- (impulse-) approximation-type calculation, where contributions are included (i) in which the observed particle is actually a high-energy spectator, and (ii) owing to the interference term between this and the usual SIA treatment[20]; (b) the double-scattering corrections[21]; and (c) the inclusion of a FSI term.[20]

It is difficult to reach conclusions about the importance of interference terms to the magnitude of the QFS peak. On the one hand, it seems that the correction factors are more prone to affect the sides of the peak in the spectra,[22] and that the measurement of the *n-p* FSI peak indicates no evidence for a strong interference with the quasifree peak. As further evidence, we have the agreement of the spectator-model calculations in the spectra in which, even for relatively high spectator energies (~2.5 MeV), no drastic deformations occur. On the other hand, the fact that the *p-p* FSI might have a significant, but nearly constant, contribution under the QFS peak would suggest that one needs to subtract the FSI "background" before drawing conclusions. A measurement in the region of low *p-p* internal energies should be able to provide useful information about the interference of *p-p* FSI and *n-p* QFS processes.

The basic difficulty with the prediction of magnitude may be in the Born approximation itself. This theory prescribes that the cross sections should be compared

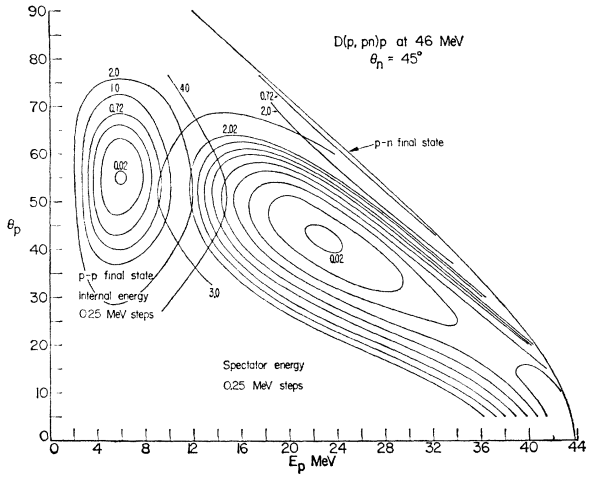

FIG. 11. Kinematical contour plot of the possible processes in the $\theta_p - E_p$ plane for $\theta_n = 45°$.

[18] R. E. Warner (private communication).
[19] E. M. Henley, F. C. Richards, and D. U. L. Yu, Nucl. Phys. **A103**, 361 (1967).
[20] A. H. Cromer and E. H. Thorndike, Phys. Rev. **131**, 1680 (1963).
[21] A. Everett, Phys. Rev. **126**, 831 (1962).
[22] M. L'Huillier, Institut de Physique Nucléaire Orsay Report No. IPNO/TH.-141, 1969 (unpublished).

at energies corresponding to the same momentum transfer. The change of that requirement in more complete theories may lead to better agreement in the Chew-Low extrapolation. An alternative way of improving the calculation might be the replacement of the term $\sigma(E, \theta)$ in Eq. (1) by the off-energy-shell scattering cross section. A series of measurements carried out at other angles where the various effects have different separations would throw light on the questions about interference, while a series carried out at a fixed set of angles at different energies both below and above the present one would be of interest, since the change of incident energy is probably the best way of moving the scattering process to different depths off the energy shell. Sets of such experiments, besides their value for the appraisal of the approximate treatment, would be helpful for a comparison with exact solutions of the proton-induced deuteron breakup developed along the lines of the recent works of Schulman[23] and of Noble.[24]

CONCLUSIONS

(1) The fact that the QFS process is strongly related to the energy of the spectator particle has been demonstrated.

(2) The shape of the measured spectra are satisfactorily fitted by the spectator model.

(3) The noncoplanar experiment demonstrates that the quasifree process tends to be coplanar except for the broadening allowed by the target internal wave function.

(4) Within the frame of the SIA approach, it has not been possible to explain the absolute cross sections. A Chew-Low extrapolation attempt is partially successful in relating the observed cross sections to the free scattering cross sections, but also indicates that other effects enter.

(5) The results should be compared with further calculations including interference and FSI terms. This will necessitate an examination of various degrees of approximation, including the Born approximation.

(6) The dependence of the cross section on off-energy-shell effects should be examined. Although there is no direct evidence that these are important, they remain an important unknown factor.

ACKNOWLEDGMENTS

It is our pleasure to express our gratitude to Dr. J. M. Cameron for help in the calculations, Dr. R. E. Warner for helpful discussion, T. Woods for participating in the measurements, and to the staff of the UCLA cyclotron for its operation of the machine.

[23] L. Schulman, Phys. Rev. **156**, 1129 (1967).
[24] J. V. Noble, Phys. Rev. **161**, 945 (1967).

PHYSICAL REVIEW VOLUME 188, NUMBER 4 20 DECEMBER 1969

^{14}N-^{14}N and ^{14}N-^{16}O Elastic Scattering*

L. A. JACOBSON†
University of Wisconsin, Madison, Wisconsin 53706

(Received 5 August 1969)

We report differential cross sections at 40–50 angles (35°–110° c.m.) for ^{14}N-^{14}N and ^{14}N-^{16}O elastic scattering. The c.m. energies vary in steps of 200 keV from 5 MeV to ~18 MeV. For ^{14}N-^{14}N, some additional data extend to ~20 MeV. Only at the lower energies does either the optical model or a modified diffraction model satisfactorily describe the data. At the higher energies, weak but broad peaks appear in the excitation curves. Evidence concerning finer structure is inconclusive.

INTRODUCTION

RECENTLY, we have made extensive measurements on ^{14}N-^{14}N and ^{14}N-^{16}O elastic scattering and have employed both a modified Blair model[1] and an optical model to describe the data. Subsequent to our analysis, other models have been proposed to describe heavy-ion elastic scattering.[2–4]

The only other data on ^{14}N-^{14}N scattering are those of Reynolds and Zucker,[5] who measured the differential

* Work supported in part by the U. S. Atomic Energy Commission.
† Present address: Schlumberger, 5000 Gulf Freeway, Houston, Tex.
[1] J. S. Blair, Phys. Rev. **95**, 1218 (1954).
[2] W. Scheid, R. Ligensa, and W. Greiner, Phys. Rev. Letters **21**, 1497 (1968).
[3] K. A. Brueckner, J. R. Buchler, and M. M. Kelly, Phys. Rev. **173**, 944 (1968).
[4] R. J. Munn, B. Block, and F. B. Malik, Phys. Rev. Letters **21**, 159 (1968); L. Rickersten, B. Block, J. W. Clark, and F. B. Malik, *ibid.* **22**, 951 (1969).
[5] H. L. Reynolds and A. Zucker, Phys. Rev. **102**, 1398 (1956).